

Transport of Lipophilic Anti-Tuberculosis Drug Benzothiazone-043 in $\text{Ca}_3(\text{PO}_4)_2$ Nanocontainers

David Rudolph,^[a] Natalja Redinger,^[b] Ulrich E. Schaible,^{*,[b]} and Claus Feldmann^{*,[a]}

Abstract: 1,3-Benzothiazin-4-one-043 (BTZ043) is a novel antimycobacterial agent for tuberculosis (TB) therapy with highly hydrophobic properties. In order to enhance local drug concentrations by improved administration and delivery to the site of the mycobacterial infection, we suggest BTZ043/Toc@Ca(ds)₂@Ca₃(PO₄)₂ nanocontainers made via a microemulsion approach for drug delivery (Toc: tocopherol; ds: dodecylsulfate). Based on our concept, the surfactant of the microemulsion itself is used to stabilize the droplet phase by interaction with Ca²⁺, followed by the formation of an inorganic Ca₃(PO₄)₂ sphere wall in one-pot reaction. Toco-

pherol (vitamin E) was used as biocompatible droplet phase of the microemulsion to dissolve the highly lipophilic BTZ043. According to electron microscopy and electron spectroscopy, the resulting BTZ043/Toc@Ca(ds)₂@Ca₃(PO₄)₂ nanocontainers exhibit an outer diameter of 28 ± 8 nm and a sphere wall of 4 ± 1 nm. The inner cavity, 18 ± 7 nm in diameter, is loaded with BTZ043 with a concentration of 30.5 µg/mL. First *in vitro* tests with murine bone marrow derived macrophages infected with *Mycobacterium tuberculosis* show promising antibiotic activity of the BTZ043/Toc@Ca(ds)₂@Ca₃(PO₄)₂ nanocontainers.

1. Introduction

Tuberculosis (TB) is the most prevalent infectious disease worldwide with 1.45 million deaths and 10 million new cases in 2019.^[1] Antimicrobial multi-resistance is an additional severe threat as illustrated by 600.000 new TB cases being mono-resistant to rifampicin and 81% of those additionally to isoniazid, two of the most important first-line anti-TB drugs.^[1] Today's search for promising drugs, e.g., via combinatorial chemistry and high-throughput screening, results in a concurrent shift of the emerging candidates to higher molecular weight and lower hydrophilicity.^[2] Concepts to combat TB and anti-bacterial resistance, therefore, not only need to explore novel anti-microbial agents, but also to make suitable drug carriers available. Thus, efficient strategies for lipophilic antibiotics to be transported in aqueous media and to cross different biological barriers are required, in order to reach sufficient concentrations of the antibiotics at the site of infection without causing adverse effects in unrelated organs.^[1,3] Mycobacteria are facultative intracellular pathogens proliferating within phagosomes of macrophages and related phagocytes. Therefore, biological barriers include the host cell


membrane, the phagosomal membrane, the inner and outer membrane of the pathogenic agent, *Mycobacterium tuberculosis* (*M.tb.*), as well as the inflammatory tissue reaction sequestering the sites of infection, the granuloma.^[3,4]

1,3-Benzothiazin-4-ones (BTZs) are a new class of antimycobacterial agents that kill *M.tb.* by inhibition of the enzyme decaprenylphosphoryl-β-d-ribose 2'-epimerase and by abolishing the decaprenylphosphoryl arabinose formation.^[5] Among these 1,3-benzothiazin-4-ones, BTZ043 is currently the most advanced agent in regard of the progress of clinical studies.^[6] Dosage schemes of lipophilic BTZ043 comprise powder aerosols for lung inhalation or tablets for gastrointestinal absorption. Powder aerosols, however, exhibit broad size distribution with a significant fraction of large particles and aggregates that do not enter the deep lung and bronchioli.^[7] Since *M.tb.*-infection is primarily a lung infection, gastrointestinal absorption is less effective due to inefficient transport to the distant lung.^[8] Efficient drug delivery concepts are therefore still highly requested. Although nanocarriers were intensely discussed for improved lung targeting,^[9] they were rarely applied for tuberculosis and so far not reported for BTZ043.

Nanoparticle-based delivery systems for lipophilic drugs, in general, often suffer from uncontrolled drug leakage and aggregation, limited cell uptake, high material complexity, unexpected toxicity and hypersensitivity, damage of cell membranes, inadequate drug loading, and/or poor stability in blood.^[1b,8a,b,10] In this regard, novel nanocarrier concepts are also highly interesting for an efficient transport and delivery of lipophilic TB antibiotics. Based on our studies related to microemulsion-made hollow nanospheres,^[9d,11] we here describe the synthesis of Ca₃(PO₄)₂ nanocontainers filled with lipophilic BTZ043 as well as the characterization of the hollow nanospheres, including a first evaluation of the antibiotic activity.

[a] M. Sc. D. Rudolph, Prof. Dr. C. Feldmann
Institute of Inorganic Chemistry, Karlsruhe Institute of Technology (KIT)
Engesserstraße 15, 76131 Karlsruhe (Germany)
E-mail: claus.feldmann@kit.edu

[b] Dr. N. Redinger, Prof. Dr. U. E. Schaible
Research Center Borstel, Leibniz Lung Center, Program Area Infections,
Dept. Cellular Microbiology, and German Center of Infection Research
(DZIF), Hamburg-Lübeck-Borstel-Riems Site
Parkallee 1–40, 23845 Borstel (Germany)
E-mail: uschaible@fz-borstel.de

 © 2020 The Authors. ChemNanoMat published by Wiley-VCH GmbH. This is an open access article under the terms of the Creative Commons Attribution Non-Commercial NoDerivs License, which permits use and distribution in any medium, provided the original work is properly cited, the use is non-commercial and no modifications or adaptations are made.

2. Results and Discussion

2.1. Synthesis and colloidal properties of BTZ043/Toc@Ca(ds)₂@Ca₃(PO₄)₂ nanocontainers

BTZ043/Toc@Ca(ds)₂@Ca₃(PO₄)₂ nanocontainers were prepared using the micellar droplets of a microemulsion as a template. Hence, a colloiddally stable oil-in-water microemulsion (*o/w*-ME) was required. Since the most common lipophilic solvents to establish microemulsion systems (e.g., hexane, octane, toluene) are of limited biocompatibility, we have used tocopherol (Figure 1a). Tocopherol—also called vitamin E—is present in many edible oils and easily metabolized by mammals. Tocopherol-based microemulsion systems have been rarely reported by now and were only recently applied for subcutaneous delivery.^[12] To stabilize the tocopherol droplet phase in water, sodium dodecylsulfate (SDS) was applied as anionic surfactant in combination with *n*-butanol as the co-surfactant (Figure 1a). Notably, an increase in the common co-surfactants, *n*-pentanol and *n*-hexanol in combination with tocopherol, only resulted in highly viscous gelatinous phases. In contrast, microemulsions with *n*-butanol and a SDS:*n*-butanol ratio around 1:2 turned out to be highly stable. Thus, optically transparent microemulsions were obtained after equilibration that show a slight yellow color originating from tocopherol (Figure 1a).

After establishing the microemulsion, BTZ043 as the active agent was dissolved in the tocopherol droplets (Figure 1b). The presence of BTZ043 is qualitatively already indicated by the characteristic red color. Such drug-loaded microemulsion droplets, however, are of limited stability in aqueous suspension since the surfactant is detached from the surface due to particle collision in suspension, which results in uncontrolled agglomeration on a timescale of about 30 min. Drug-loaded microemulsion droplets are known to be even less appropriate for physiological use due to their low stability in cell culture media and blood, uncontrolled drug leakage and aggregation of the lipophilic drug, unexpected cellular toxicity and hypersensitivity as well as damaging of cell membranes.^[3,8c,13] Therefore, the BTZ043/tocopherol droplets were stabilized by an inorganic

Ca₃(PO₄)₂ shell (Figure 1c,d). Beside the stabilization of the lipophilic droplet phase, the addition of Ca²⁺ was chosen for several reasons. On the one hand, Ca(ds)₂ (ds: dodecylsulfate) as well as Ca₃(PO₄)₂ are insoluble in water at neutral pH. On the other hand, calcium and phosphate can be considered as less harmful and highly biodegradable. To control the synthesis and formation of the inorganic nanocontainer, first of all, a solution of Ca(Ac)₂ was added to the microemulsion system. By ionic interaction Ca²⁺ coordinates to the sulfate groups of ds and reduces the thermal motion of the surfactant (Figure 1c). After equilibration, an aqueous solution of Na₂(HPO₄) was slowly added, which initiates slow formation of a Ca₃(PO₄)₂ shell (Figure 1d). The formation of the Ca₃(PO₄)₂ shell is optically indicated by the brightening of the BTZ043-induced red color. This color change is driven by the reflection of daylight from the outer colorless Ca₃(PO₄)₂ shell (Figure 1d).

The course of the reaction and specifically the modification of the particle surface can be also followed by measuring the Zeta potential (Figure 2a). The ds-stabilized microemulsion exhibits a highly negative charge of −95 to −100 mV at pH 5 to 12. After addition of Ca²⁺, the surface charge is much less negative (−35 to −45 mV). Now, there is also a stronger influence of the pH on the surface charge, which can be ascribed to the protonation/deprotonation of H₂O molecules coordinated to Ca²⁺ on the side of the solution. Moreover, the cation termination results in a precipitation of the nanoparticles after some minutes (Figure 1c), whereas the ds-stabilized microemulsion and the final nanocontainers remain colloiddally stable over several weeks (Figure 1b,d). Subsequent to the formation of the Ca₃(PO₄)₂ shell, the BTZ043/Toc@Ca(ds)₂@Ca₃(PO₄)₂ nanocontainers do not show considerable change of the surface charge (−35 to −55 mV) in comparison to BTZ043/Toc@Ca(ds)₂ (−35 to −45 mV) However, the course of the surface charge with highest negative charging at pH 12 and a continuous decrease of the charge at more acidic pH is characteristic for phosphates^[14] and fits with calcium phosphate as outer shell of the nanocontainers (Figure 2a). After purification, colloiddally highly stable suspensions of BTZ043/Toc@Ca(ds)₂@Ca₃(PO₄)₂ nanocontainers were obtained. The yellow suspensions do not

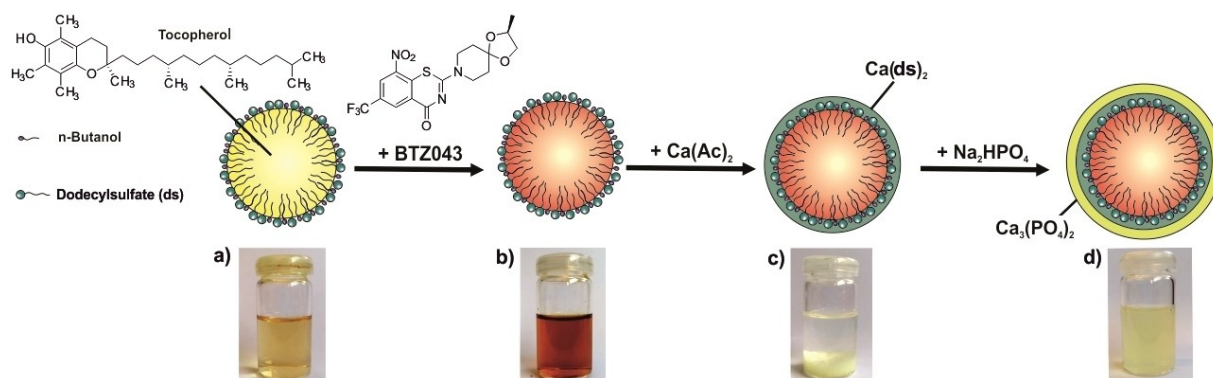


Figure 1. Scheme illustrating the synthesis of BTZ043/Toc@Ca(ds)₂@Ca₃(PO₄)₂ nanocontainers: a) *o/w*-Microemulsion with tocopherol as lipophilic droplet phase, ds as the surfactant and *n*-butanol as the co-surfactant; b) Microemulsion with a saturated solution of BTZ043 in tocopherol as lipophilic droplet phase; c) Stabilization of droplet phase by formation of Ca(ds)₂; d) Formation of the outer inorganic Ca₃(PO₄)₂ shell.

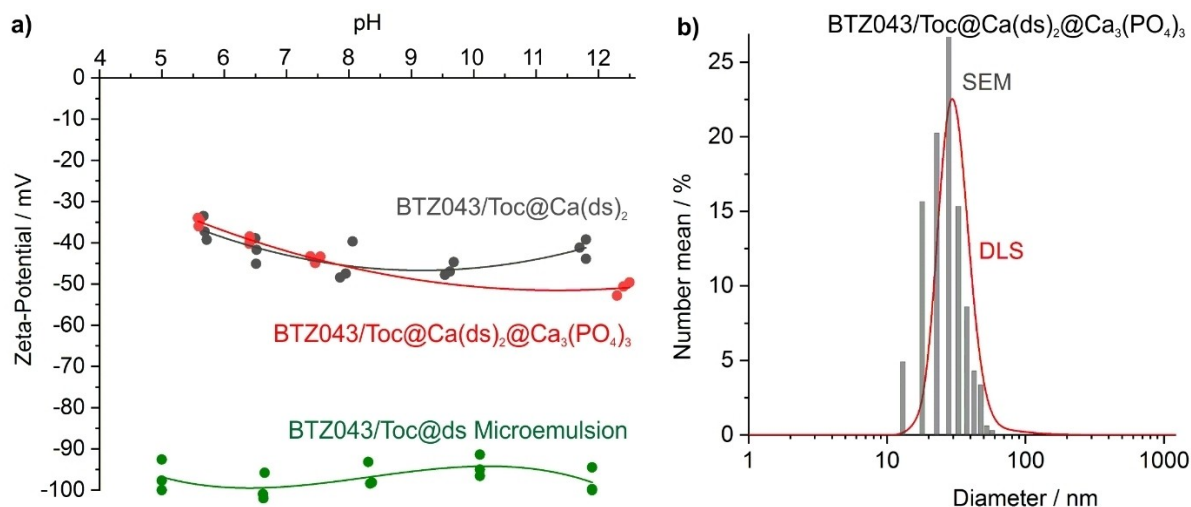


Figure 2. Colloidal properties of the BTZ043/Toc@Ca(ds)₂@Ca₃(PO₄)₂ nanocontainers: a) Zeta potential in relation to the different steps of the synthesis; b) Particle size distribution according to DLS and SEM.

show any sedimentation over a timescale of several weeks. Finally, dynamic light scattering (DLS) indicates a mean hydrodynamic particle size of 30 ± 6 nm (Figure 2b), which is well in agreement with the mean particle size obtained from statistical evaluation of > 150 particles on scanning electron microscopy (SEM) images (27 ± 4 nm).

2.2. Composition of BTZ043/Toc@Ca(ds)₂@Ca₃(PO₄)₂ nanocontainers

The chemical composition of the as-prepared BTZ043/Toc@Ca(ds)₂@Ca₃(PO₄)₂ nanocontainers was characterized by X-ray powder diffraction (XRD), Fourier-transformed infrared spectroscopy (FT-IR), thermogravimetry (TG), and elemental analysis (EA) (Figure 3). According to XRD, the nanocontainers are amorphous for the most part, which is expected for metal phosphates prepared at ambient temperature.^[15] Two very weak and broad peaks nevertheless indicate the presence of Ca₁₀(PO₄)₆(OH)₂ (Figure 3a). FT-IR predominately confirms the presence of phosphate ($\nu(\text{P}=\text{O})$: 1150–1050 cm⁻¹) and ds ($\nu(\text{S}=\text{O})$: 1300–1200 cm⁻¹) (Figure 3b). The vibrations of BTZ043 are less characteristic due to its low concentration relative to tocopherol and Ca₃(PO₄)₂ and due to partial overlay with other vibrations. Finally, EA allows determining the C/H/N/S contents and results in 40.7% C, 6.2% H, 0.3% N and 3.6% S. Hereof, the N content is indicative for BTZ043, so that a BTZ043 load of 3.1 mg per 100 mg for the BTZ043/Toc@Ca(ds)₂@Ca₃(PO₄)₂ nanocontainers can be deduced. Total organics combustion determined by TG shows two step decomposition with a first step at 50–150 °C (12 wt-%) and a second step at 150–500 °C (63 wt-%) (Figure 3c). The first decomposition can be related to the release of water from the nanocontainers, whereas the second step denotes the thermal decomposition of all organic compounds, including ds, tocopherol and BTZ043. The thermal remnant with a solid residue of only 25 wt-% was identified as

mixture of Ca₃(PO₄)₂ and Ca₁₀(PO₄)₆O (Figure 3d). These finding reflects the low thickness of the Ca₃(PO₄)₂ sphere wall in comparison to the total volume of the BTZ043/Toc@Ca(ds)₂@Ca₃(PO₄)₂ nanocontainers.

To determine the concentration of the encapsulated BTZ043 in BTZ043/Toc@Ca(ds)₂@Ca₃(PO₄)₂ nanocontainers, UV-VIS spectroscopy was applied (Figure 4). To this concern, a calibration curve of BTZ043 dissolved in ds-stabilized BTZ043/Toc microemulsions at known concentrations was measured (Figure 4b). This calibration curve shows an almost ideal linear dependence between absorbance and BTZ043 concentration in a range of 0–40 µg/mL. Using the Lambert-Beer equation is therefore appropriate to determine the BTZ043 concentration in the nanocontainers. Since the measurements were performed in a reflecting sphere (Ulbricht sphere), the scattering of the nanocontainers is not an issue. As a result of the photometrical quantification, the as-prepared suspensions contain the nanocontainers with a concentration of $c(\text{NP}) = 1$ mg/mL and BTZ043 with a concentration of $c(\text{BTZ043}) = 30.5$ µg/mL. This finding is in good agreement with the results from elemental analysis (3.2 mg BTZ043 per 100 mg of the nanocontainers).

2.3. Structure of BTZ043/Toc@Ca(ds)₂@Ca₃(PO₄)₂ nanocontainers

The structure of the as-prepared BTZ043/Toc@Ca(ds)₂@Ca₃(PO₄)₂ nanocontainers was characterized based on electron microscopy, including SEM, scanning transmission electron microscopy (STEM) and high-resolution transmission electron microscopy (HRTEM). Accordingly, SEM shows a mean diameter of 28 ± 8 nm (Figure 5a,b), which is well in agreement with the mean hydrodynamic diameter obtained by DLS analysis (30 ± 13 nm, Figure 2b). In addition to size characterization based on a statistically relevant great number of nanocontainers via DLS and SEM, STEM images of nanocontainers at high magnification

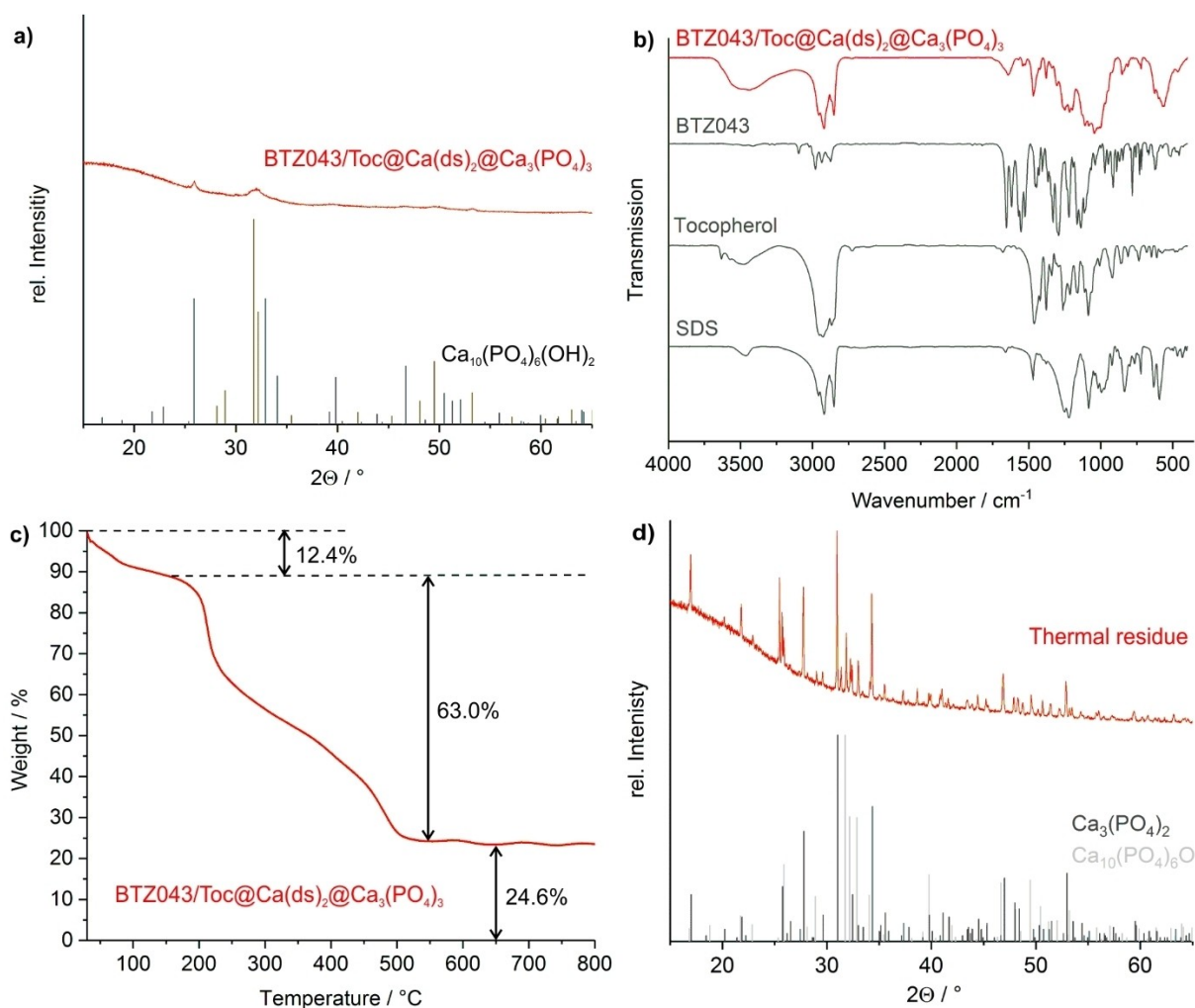


Figure 3. Chemical composition of the BTZ043/Toc@Ca(ds)₂@Ca₃(PO₄)₂ nanocontainers: a) XRD of as-prepared sample (reference: ICDD-No. 00-064-0738: Ca₁₀(PO₄)₆(OH)₂); b) FT-IR of as-prepared sample with ds, tocopherol and BTZ043 as references; c) TG of as-prepared sample; d) XRD of thermal remnant after TG analysis (references: ICDD-No. 00-055-0898: Ca₃(PO₄)₂; ICDD-No. 01-089-6489: Ca₁₀(PO₄)₆O).

confirm the outer particle diameter and—even more important—the presence of the inner cavity in the BTZ043/Toc@Ca(ds)₂@Ca₃(PO₄)₂ nanocontainers (Figure 5c,d). Accordingly, the significantly lower electron absorption validates the inner cavity with a diameter of 18 ± 7 nm and the surrounding sphere wall with a thickness of about 4 ± 1 nm (Figure 5d).

In addition to SEM, it was of course intended to perform TEM analysis of the nanocontainers. However, TEM analysis of the as-prepared BTZ043/Toc@Ca(ds)₂@Ca₃(PO₄)₂ nanocontainers failed since the nanoparticles were completely destroyed in the electron beam within few seconds. This finding can be employed by using the acceleration voltage applied by SEM (20 kV) and TEM (200 kV) to estimate the stability of the nanocontainers. Due to the significantly higher kinetic energy of the electrons as well as the resulting warming and charging, the nanocontainers are stable enough under SEM conditions but not under TEM conditions. Taking the non-conducting nature of the nanocontainers, 28 ± 8 nm in diameter, and the presence of an inorganic shell with a thickness of only 4 ± 1 nm

and 18 ± 7 nm of a decomposable organic inner cavity into account, the rapid decomposition of the BTZ043/Toc@Ca(ds)₂@Ca₃(PO₄)₂ nanocontainers under TEM conditions is not a surprise.

To perform TEM analysis, we have modified the synthesis in order to realize in principle identical nanocontainers, however, with a larger diameter and a thicker sphere wall. In this regard, specifically the SDS:Ca(Ac)₂:Na(H₂PO₄) ratio was modified to 1.0:20.4:10.5 with significantly higher amounts of calcium and phosphate (instead of SDS:Ca(Ac)₂:Na₂(HPO₄) = 1.0:5.3:2.6 for the aforementioned small-sized nanocontainers). These modified, larger BTZ043/Toc@Ca(ds)₂@Ca₃(PO₄)₂ nanocontainers were then examined by TEM and energy-dispersive X-ray spectroscopy (EDXS) (Figures 6,7). Whereas the diameter of the inner cavity of the modified BTZ043/Toc@Ca(ds)₂@Ca₃(PO₄)₂ nanocontainers increased only slightly to 39 ± 15 nm, the thickness of the Ca₃(PO₄)₂ wall was significantly increased to 27 ± 7 nm (Figures 6a). As a consequence, the outer diameter of the modified BTZ043/Toc@Ca(ds)₂@Ca₃(PO₄)₂ nanocontainers was

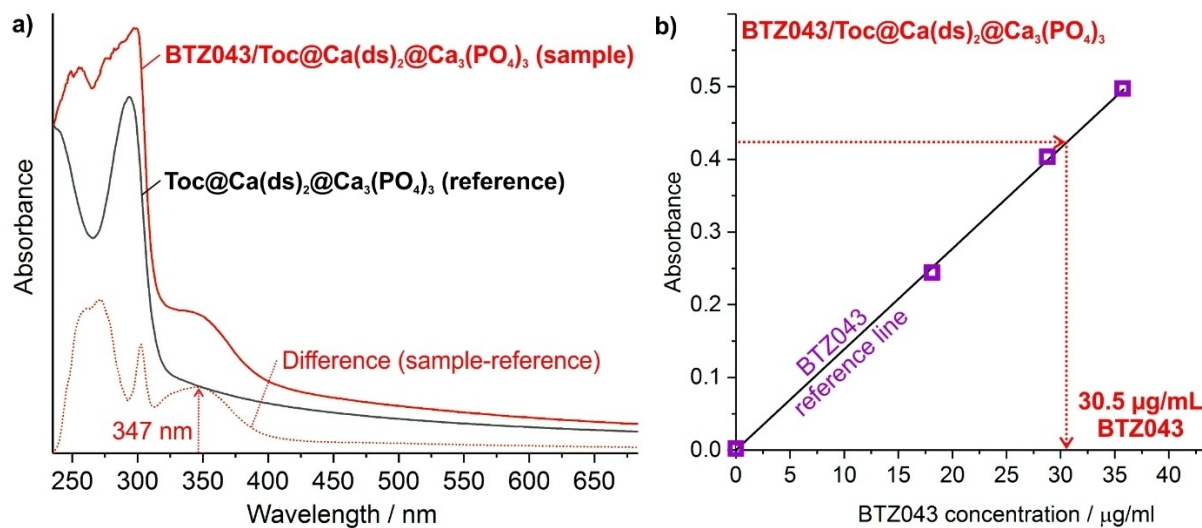


Figure 4. Photometrical analysis of BTZ043/Toc@Ca(ds)₂@Ca₃(PO₄)₂ nanocontainers: a) UV-VIS spectra of BTZ043/Toc@Ca(ds)₂@Ca₃(PO₄)₂ suspension (samples) and Toc@Ca(ds)₂@Ca₃(PO₄)₂ suspension (reference) as well as difference of both curves (suspensions with $c(\text{nanocontainers}) = 1.0 \text{ mg/mL}$); b) UV-VIS calibration curve for BTZ (ds-stabilized BTZ043/Toc microemulsions) with absorbance measured at $\lambda = 347 \text{ nm}$ (pink dots represent the measured values; black line represents the linear fitting function).

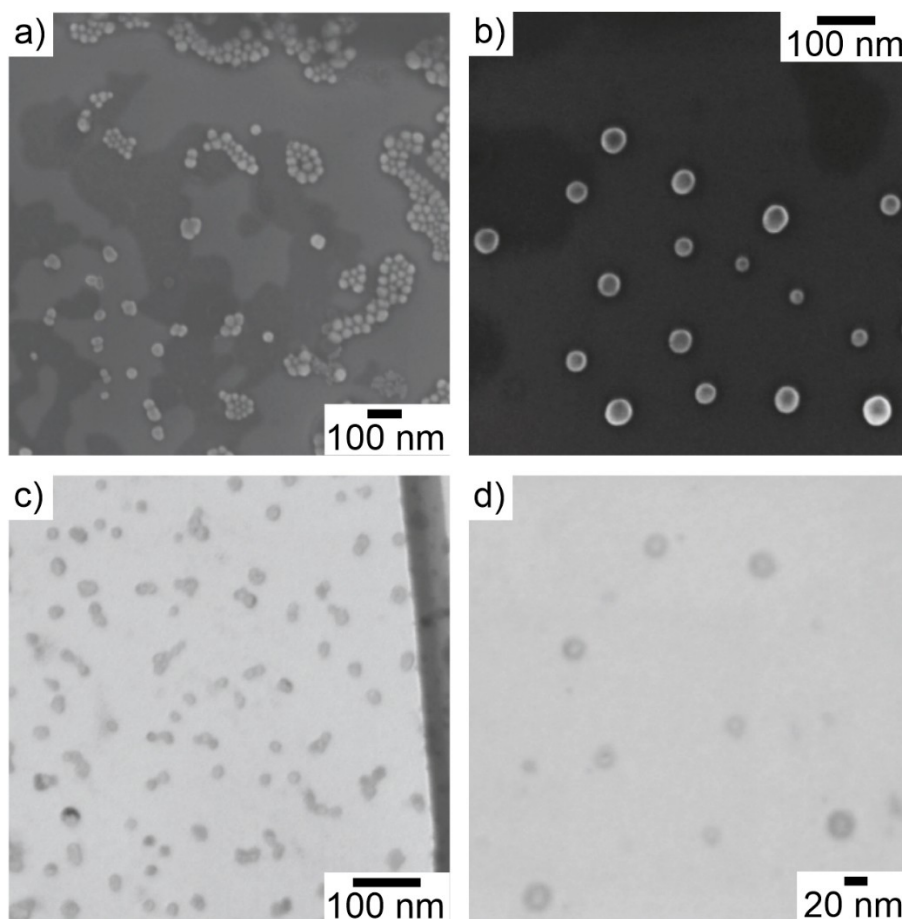


Figure 5. Electron microscopic characterization of BTZ043/Toc@Ca(ds)₂@Ca₃(PO₄)₂ nanocontainers: a + b) SEM images at different levels of magnification; c + d) STEM images at different levels of magnification.

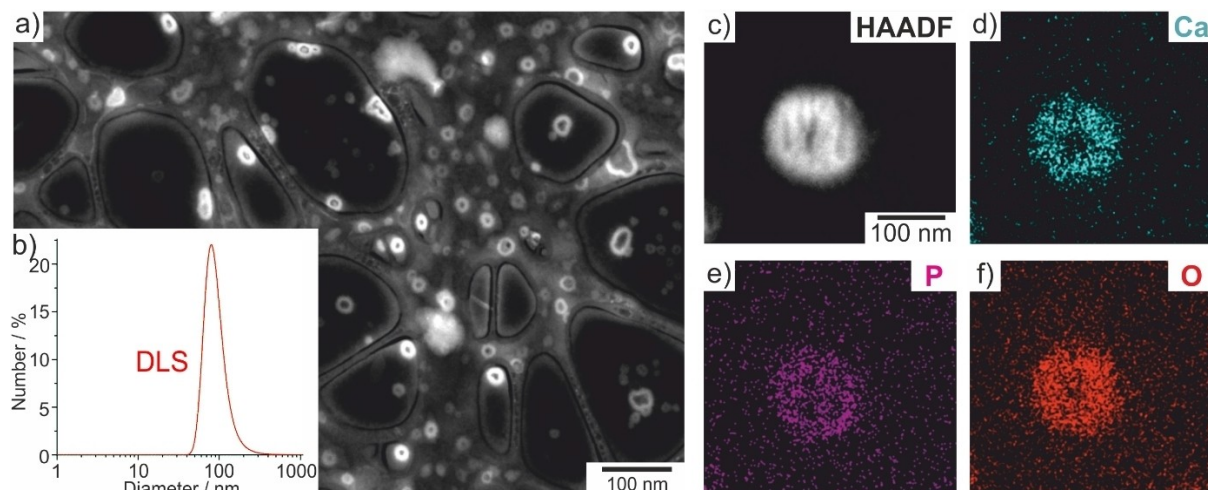


Figure 6. Modified (larger) BTZ043/Toc@Ca(ds)₂@Ca₃(PO₄)₂ nanocontainers: a) STEM overview image; b) DLS of aqueous suspension; c) HAADF-STEM image of selected nanocontainer; d–e) EDXS of the nanocontainer on HAADF-STEM image (d) with element mappings of Ca (d), P (e), O (f).

increased to 80 ± 20 nm. In addition, the size distribution became broader as compared to the original small-sized nanocontainers.

EDXS element mappings of the modified, larger BTZ043/Toc@Ca(ds)₂@Ca₃(PO₄)₂ show a homogenous distribution of calcium, phosphorus and oxygen all over the nanocontainers (Figures 6). The presence of an inner cavity with an outer Ca₃(PO₄)₂ shell was confirmed by HAADF-STEM images (Figure 6) as well as by the EDXS element mappings (especially in the case of calcium, Figure 6d). Here, it needs to be noticed that element mappings of fluorine and sulfur, potentially indicating BTZ043 and ds, did not result in reliable intensities in regard of the significance of the measurement. This can be ascribed to the low concentration in the liquid phase in comparison to the significantly higher density of the respective elements per volume in the solid Ca₃(PO₄)₂ wall. The presence of the inner cavity is even more obvious when performing EDXS line scans

(Figures 7a). Determining the concentration of Ca, P and O along the orange line on the HAADF-STEM image shows a characteristic dip in the center of the nanocontainer (Figures 7b). This lower concentration of Ca, P and O indicates the inner cavity of the nanocontainer since the electron beam only passes through bottom and ceiling of the nanocontainer. In contrast, EDXS line scans point to a maximum concentration of Ca, P and O if the electron beam cuts through the side of the nanocontainer (Figures 7b). Altogether, HRTEM and EDXS analysis of the modified, larger BTZ043/Toc@Ca(ds)₂@Ca₃(PO₄)₂ clearly point to the presence of nanocontainers with an inner cavity. In terms of biomedical use, the small-sized nanocontainers with an outer diameter of 28 ± 8 nm are of course much more interesting (Figure 5).

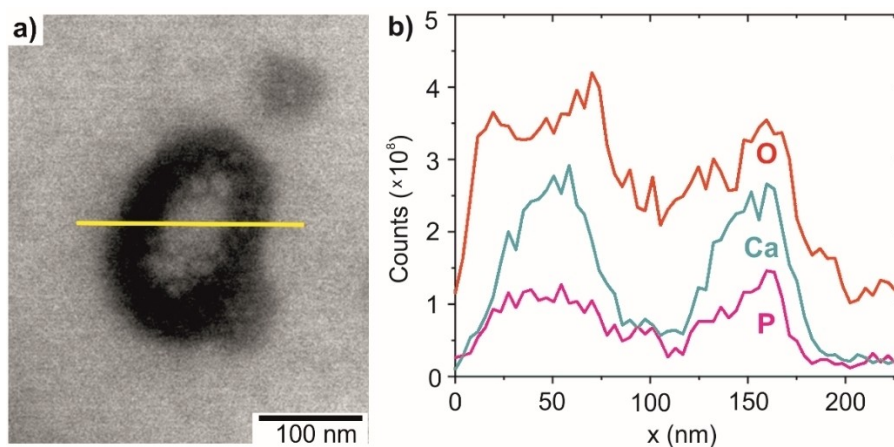


Figure 7. EDXS line scan of modified (larger) BTZ043/Toc@Ca(ds)₂@Ca₃(PO₄)₂ nanocontainers: a) HAADF-STEM image; b) EDXS line scan of nanocontainer on HAADF-STEM image (a) along the orange line indicating the element distribution of Ca, P, O.

2.4. Antibiotic activity of BTZ043/Toc@Ca(ds)₂@Ca₃(PO₄)₂ nanocontainers

To verify the feasibility of our nanocontainer concept as a proof-of-the-concept, murine bone marrow derived macrophages (BMMO) infected with *M.tb.* were used to assess anti-mycobacterial activity by determining colony forming units (CFU) (Figure 8a). Anti-mycobacterial activities were assessed in BMMO infected with *M.tb.* for 2 hours and subsequently incubated with the compounds at 37 °C/7.5% CO₂ atmosphere for 48 and 72 hours before cells were lysed. Cells were treated with either BTZ043/Toc@Ca(ds)₂@Ca₃(PO₄)₂ nanocontainers in aqueous suspension, BTZ alone (stock solution pre-dissolved in DMF, positive control), empty Toc@Ca(ds)₂@Ca₃(PO₄)₂ nanocontainers that did not contain BTZ043 (aqueous suspension, negative control) or were left non-treated (negative control) (Figure 8b,c). The dilutions as indicated in Figures 8b and c were adjusted to BTZ043 concentration equivalents.

Toc@Ca(ds)₂@Ca₃(PO₄)₂ reference nanocontainers did not affect mycobacterial growth, which was similar to non-treated

cells as indicated by similar numbers of colony forming units (CFU). The viability of the macrophage monolayers was neither affected by empty nor by BTZ043-free nanocontainers, which indicates that the nanocontainers as such—including tocopherol, ds as the surfactant, and Ca₃(PO₄)₂ as the inorganic shell—did not cause any observable cytotoxic effects even in infected cells (data not shown). However, BTZ043/Toc@Ca(ds)₂@Ca₃(PO₄)₂ nanocontainers show anti-mycobacterial efficacy at 1 and 0.1 µg/ml concentrations comparable to free BTZ043 (solution in DMF, Figure 8b,c). Thus, BTZ043 has the same antibiotic activity at comparable concentrations although encapsulated in nanocontainers. Since the uptake into infected cells is a much less complex mechanism in cell cultures *in vitro* as compared to the situation *in vivo*, where drugs additionally need to enter the infectious sites, i.e., by crossing the granuloma barrier, this result is highly promising as the nanocontainers may exhibit activity identical to the dissolved, free drug. *In vivo* drug efficacy studies using *M. tb.*-infected mice, however, require high safety levels and complex experimental set-ups (broad range of doses,

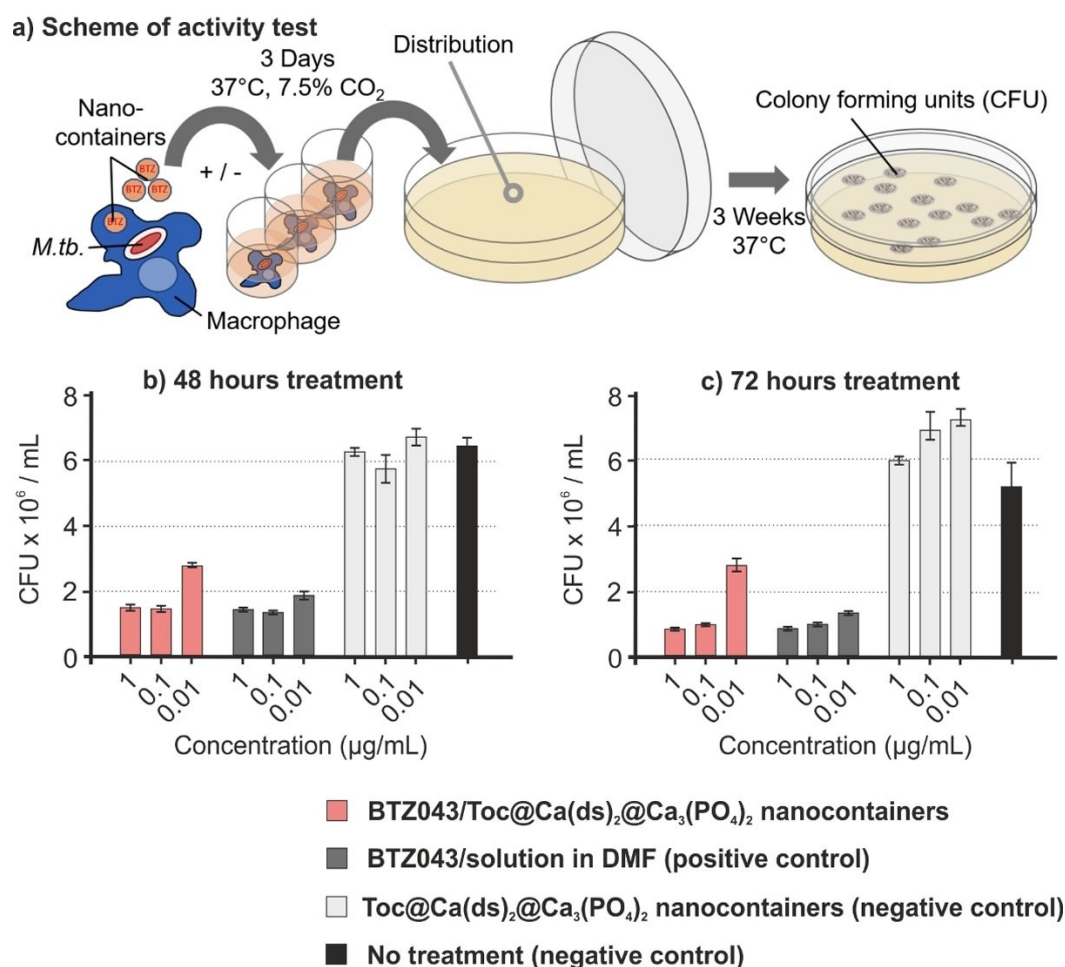


Figure 8. Antibiotic activity of BTZ043/Toc@Ca(ds)₂@Ca₃(PO₄)₂ nanocontainers against intracellular *M. tb.*: a) Schematic drawing of antibiotic activity tests in *M.tb.* H37Rv infected macrophages by determining colony forming units (CFU). Data shown represent the means \pm standard deviations from three technical triplicates representing three independent equivalent biological replica experiments; b + c) Assessment of CFU for the nanocontainers in BMMO infected with *M. tb.* for 2 h and subsequent incubation for b) 48 hours and c) 72 hours with solution of BTZ in DMF (positive control), Toc@Ca(ds)₂@Ca₃(PO₄)₂ nanocontainers (negative control) and non-treated intracellular *M. tb.* (negative control).

adjustment of various host parameters), which is beyond this *in vitro* proof-of-concept study.

3. Conclusions

BTZ043/Toc@Ca(ds)₂@Ca₃(PO₄)₂ nanocontainers filled with the lipophilic anti-tuberculosis drug 1,3-benzothiazin-4-one-043 (BTZ043) were prepared via a microemulsion strategy. The microemulsion was established with water as the dispersant phase, tocopherol as the lipophilic droplet phase and dodecylsulfate (ds) as anionic surfactant. Tocopherol (vitamin E) was chosen as biocompatible oil phase and used to dissolve BTZ043. The micellar system was stabilized first by addition of Ca²⁺, which coordinates to the sulfate groups of ds and thereby reduces the thermal motion of the surfactant. Thereafter, Na₂(HPO₄) was slowly added to allow the formation of a Ca₃(PO₄)₂ shell around the former micellar droplet, which results in BTZ043/Toc@Ca(ds)₂@Ca₃(PO₄)₂ nanocontainers.

The composition of the nanocontainers was validated by different analytical tools (XRD, FT-IR, UV-Vis, Zeta potential analysis, thermogravimetry, elemental analysis, electron microscopy). Optical spectroscopy as well as elemental analysis confirm a BTZ043 load of 3.1 mg BTZ043 per 100 mg of the nanocontainers. Electron microscopy (SEM, TEM) and electron spectroscopy (EDXS) validate the nanocontainer structure with an outer diameter of 28 ± 8 nm, a sphere wall of 4 ± 1 nm and an inner cavity of 18 ± 7 nm. Upon variation of the SDS:Ca (Ac)₂:Na₂(HPO₄) ratio, the size can be modified resulting in larger nanocontainers with an outer diameter of 80 ± 20 nm, a wall thickness of 27 ± 7 nm and an inner cavity of 39 ± 15 nm.

First *in vitro* tests in *M.tb.*-infected macrophages treated with BTZ043/Toc@Ca(ds)₂@Ca₃(PO₄)₂ nanocontainers in comparison to BTZ (positive control) and BTZ-free nanocontainers (negative control) indicate the novel BTZ043/Toc@Ca(ds)₂@Ca₃(PO₄)₂ nanocontainers to be as active as BTZ043 alone. On the one hand, this validates the feasibility of the nanocontainer concept, and on the other hand, this indicates the BTZ043/Toc@Ca(ds)₂@Ca₃(PO₄)₂ as promising shuttles to transport lipophilic drugs.

Experimental Section

Synthesis details

General aspects. Sodium dodecylsulfate (SDS, ≥99.0%, Sigma-Aldrich, Germany), *n*-butanol (>99.5%, Riedel-de-Haën, Germany), α-tocopherol (97%, ABCR, Germany), Na(H₂PO₄)×H₂O (99.5%, Riedel-de-Haën), Na₂(HPO₄)×2H₂O (99%, Riedel-de-Haën), disodium citrate (99%, Sigma-Aldrich), citric acid (99.5%, Sigma-Aldrich), calcium acetate (>99%, Sigma-Aldrich), and benzothiazinone-043 (99.66%, MedChemExpress, Germany) were used as purchased.

Formation of the microemulsion. A colloidally stable oil-in-water microemulsion (o/w-ME) was established by mixing 2.5 mL (140 mmol) of demineralized water as the polar dispersant phase, 0.4 mL (0.38 g, 0.88 mmol) of tocopherol (Toc) as the lipophilic droplet phase, 700 mg (2.43 mmol) of sodium dodecylsulfate (SDS)

as the surfactant and 0.45 mL (0.36 g, 4.91 mmol) of *n*-butanol as the co-surfactant. It needs to be noticed that the much more common co-surfactants *n*-pentanol and *n*-hexanol in combination with tocopherol only result in highly viscous gelatinous phases. In contrast, microemulsions with *n*-butanol and a SDS:*n*-butanol ratio around 1:2 turned out highly stable. Thus, a yellow, transparent microemulsion was obtained. Thereafter, 27.2 mg BTZ043 were dissolved in the microemulsion, resulting in a color change from yellow to red. Thereafter, 0.8 mL of the as-prepared microemulsion, containing 140 mg (0.48 mmol, 1 eq) of SDS, 5.4 mg of BTZ043 and 0.08 mL (0.08 g, 0.17 mmol) of Toc were diluted with demineralized water to a total volume of 5 mL and allowed to equilibrate for 30 min.

Formation of BTZ043/Toc@Ca(ds)₂@Ca₃(PO₄)₂ nanocontainers. A solution of 400 mg (2.53 mmol, 5.3 eq) of calcium acetate and 30 mg (0.16 mmol) of citric acid in 50 mL of water was adjusted to pH 10 upon addition of 0.1 M NaOH. The aforementioned diluted microemulsion was slowly added to this solution with a syringe pump over a period of 30 min. The resulting reddish suspension was stirred for 1 hour and then centrifuged (15,000 rpm, 15 min). Thereafter, the nanocontainers were redispersed in 50 mL of demineralized water and the pH of the suspension adjusted to pH 10 upon addition of 0.1 M NaOH. Finally, a solution of 225 mg (1.26 mmol, 2.62 eq) of Na₂(HPO₄) in 5 mL of demineralized water was added via a syringe pump over a period of 30 min. The resulting suspension was centrifuged (25,000 rpm, 15 min), redispersed in water and again centrifuged (25,000 rpm, 15 min). Thereafter, the BTZ043/Toc@Ca(ds)₂@Ca₃(PO₄)₂ nanocontainers can be redispersed in 8.46 mM solution of disodium citrate or dried to obtain powder samples.

Formation of the microemulsion to obtain larger nanocontainers. The microemulsion was prepared as described above. Instead of 0.8 mL of the as-prepared microemulsion, however, only 0.2 mL of the as-prepared microemulsion, containing 35 mg (0.12 mmol, 1 eq) of SDS, 1.35 mg of BTZ043 and 0.02 mL (0.02 g, 0.043 mmol) of Toc were added to a solution of 225 mg (1.26 mmol, 10.3 eq) of Na (H₂PO₄) and 30 mg (0.16 mmol) of citric acid in 50 mL of water. Upon addition of 0.5 M NaOH the solution was adjusted to pH 6.1. Thereafter, 338 mg (2.45 mmol, 20.4 eq) of Ca(Ac)₂ in 5 mL of water were added dropwise. The solution slowly turned to a colorless turbid suspension. This suspension was stirred for additional 4 hours and then gradually heated to 80 °C within 3 hours. Prolonged stirring and slow heating support dehydration and densification of the Ca₃(PO₄)₂ shell, which is indicated by a slow decrease of the pH value from 6.1 to 5.1 according to the following reaction: 3Ca²⁺ + 2[H₂PO₄]⁻ → Ca₃(PO₄)₂ + 4H⁺. Finally, the nanocontainers were purified by centrifugation, followed by redispersion in and centrifugation from demineralized water, which was performed twice to remove all salts and residual starting materials. Thereafter, the nanocontainers can be redispersed in water or dried to obtain powder samples.

Analytical equipment

Scanning electron microscopy (SEM). Scanning electron microscopy (SEM) was carried out with a Zeiss Supra 40 VP microscope (Zeiss, Germany), equipped with a Schottky field emitter (2.0 nm resolution). To this concern, diluted aqueous suspensions of the BTZ043/Toc@Ca(ds)₂@Ca₃(PO₄)₂ nanocontainers were deposited on silicon wafers and left for drying overnight. The acceleration voltage was in the range of 5–13 kV and the working distance was 2–3 mm. Average particle diameters were calculated by statistical evaluation of at least 150 nanoparticles (ImageJ 1.47v software).

Transmission electron microscopy (TEM). Transmission electron microscopy (TEM) and high-angle annular dark-field scanning transmission electron microscopy (HAADF-STEM) were conducted with a FEI Osiris microscope at 200 kV (FEI, The Netherlands). TEM samples were prepared by evaporating aqueous suspensions of the BTZ043/Toc@Ca(ds)₂@Ca₃(PO₄)₂ nanocontainers on amorphous carbon (Lacey-)film suspended on copper grids. Average particle diameters were calculated by statistical evaluation of at least 150 nanoparticles (ImageJ 1.47v software).

Energy-dispersive X-ray (EDX) spectroscopy. High-resolution EDXS was performed to analyze the chemical composition of single BTZ043/Toc@Ca(ds)₂@Ca₃(PO₄)₂ nanocontainers. The spectra were obtained at 200 kV electron energy with a FEI Osiris microscope that was equipped with a Bruker Quantax system (XFlash detector, Bruker, Germany). EDX spectra were quantified with the FEI software package "TEM imaging and analysis" (TIA). Using TIA, element concentrations were calculated on the basis of a refined Kramers' law model that includes corrections for detector absorption and background subtraction. Standardless quantification, i.e. by means of theoretical sensitivity factors, without thickness correction was applied. EDX spectra were taken in the STEM mode with a probe diameter of 0.5 nm. Using a focused electron probe, EDXS area scans were performed to obtain average compositions of larger sample regions. The EDX spectra were acquired by continuously scanning the electron probe in the pre-defined region.

Dynamic light scattering (DLS). DLS was used to determine the hydrodynamic diameter of the as-prepared BTZ043/Toc@Ca(ds)₂@Ca₃(PO₄)₂ nanocontainers in the suspensions. Studies were conducted at room temperature in glass or polystyrene cuvettes applying a Nanosizer ZS (Malvern Instruments, United Kingdom).

X-ray powder diffraction (XRD). X-ray powder diffraction (XRD) was performed with a Stoe STADI-MP diffractometer (Stoe, Germany) operating with Ge-monochromatized Cu-K α -radiation ($\lambda = 1.54178 \text{ \AA}$) and Debye-Scherrer geometry. The dried BTZ043/Toc@Ca(ds)₂@Ca₃(PO₄)₂ nanocontainers were fixed between Scotch tape and acetate paper and measured between -69° and $+69^\circ$ of two-theta.

Fourier-transformed infrared spectroscopy (FT-IR). Fourier-transformed infrared spectroscopy (FT-IR) was performed on a Bruker Vertex 70 FT-IR spectrometer (Bruker, Germany). All BTZ043/Toc@Ca(ds)₂@Ca₃(PO₄)₂ nanocontainers samples were pestled and diluted with KBr (3 mg of sample per 300 mg of KBr) and pressed to pellets.

Elemental analysis (C/H/N/S analysis). Elemental analysis (C/H/N/S analysis) was performed via thermal combustion with an Elementar Vario Microcube device (Elementar, Germany) at a temperature of about 1100 °C.

Optical spectroscopy (UV-Vis spectroscopy). UV-Vis spectroscopy was used to quantify the amount of BTZ in the respective BTZ043/Toc@Ca(ds)₂@Ca₃(PO₄)₂ nanocontainers according to the Kubelka-Munk formalism. The respective concentrations were quantified in comparison to reference solutions with known concentration by applying a calibration curve. UV-VIS spectra were recorded with an UV2700 from Shimadzu (Japan). Nanoparticle suspensions were measured in quartz glass cells (Starna, type Q, 170–2700 nm, spectral quality 6) in an integrating sphere in diffuse transmission geometry against the corresponding pure solvent as a reference.

In vitro studies

M. tuberculosis-infected macrophages. Bone marrow (BM) was flushed out of the femur and tibia of C57BL/6 mice using ice-cold complete DMEM (high glucose DMEM Dulbecco's modified eagle

medium supplemented with 10% FCS, 10 mM HEPES, 2 mM L-glutamine, 50 ng/mL M-CSF; Sigma-Aldrich). Single cell suspensions were cultured for 7 days at 37 °C with 5% CO₂. At day 7, differentiated macrophages were harvested by flushing with ice-cold PBS, counted, adjusted to 10⁶ cells/mL, seeded in 48-well cell culture plates (Sarstedt, Germany), and used for further experiments.

M. tuberculosis H37Rv was harvested by centrifugation at 1000×g for 10 min. The bacterial pellet was resuspended in DMEM and centrifuged for another 10 min at 1500×g. The supernatant was exchanged by fresh medium and flushed 4-times through a 23G needle (BD Pharmingen, San Diego, USA), adjusted against cell culture media to an optical density (OD) at 600 nm of 0.5, and used 1 in 10 diluted in cell culture medium for infection of BMMO. Cells were infected for 2 h at 37 °C, 7.5% CO₂ with *M. tuberculosis*. After washing, the cells were further incubated with BTZ043/Toc@Ca(ds)₂@Ca₃(PO₄)₂ nanocontainers and the respective control compounds. After 48 and 72 h of incubation, BMMO were lysed in water containing 01% bovine albumin and 0.1% Tween80. Lysates were diluted and plated onto 7H11 agar plates. After 3 weeks of incubation at 37 °C, colony forming units were counted (see schematic drawing in Figure 8a).

Acknowledgements

The authors thank the group of Prof. Dr. D. Gerthsen for excellent cooperation in regard of electronic microscopic characterization, and Kristine Hagens for expert technical assistance. Moreover, the authors acknowledge the German Federal Ministry of Education and Research (BMBF) for funding within the joint research project ANTI-TB. Finally, the authors are grateful to the German Research Society (DFG) for funding of analytical equipment. Open access funding enabled and organized by Projekt DEAL.

Conflict of Interest

The authors declare no conflict of interest.

Keywords: Nanocontainer · calcium phosphate · benzothiazone-043 · antibiotics · tuberculosis

- [1] *Reviews:* a) World Health Organization (WHO), *Global tuberculosis report 2019*, ISBN 978-92-4-156571-4; b) M. J. A. Reid, N. Arinaminpathy, A. Bloom, B. R. Bloom, C. Boehme, R. Chaisson, D. P. Chin, G. Churchyard, H. Cox, L. Ditiu, M. Dybul, J. Farrar, A. S. Fauci, E. Fekadu, P. I. Fujiwara, T. B. Hallett, C. L. Hanson, M. Harrington, N. Herbert, P. C. Hopewell, C. Ikeda, D. T. Jamison, A. J. Khan, I. Koek, N. Krishnan, A. Motsaedi, M. Pai, M. C. Raviglione, A. Sharman, P. M. Small, S. Swaminathan, Z. Temesgen, A. Vassall, N. Venkatesan, K. van Weezenbeek, G. Yamey, B. D. Agins, S. Alexandru, J. R. Andrews, N. Beyeler, S. Bivol, G. Brigden, A. Cattamanchi, D. Cazabon, V. Crudu, A. Daftary, P. Dewan, L. K. Doepel, R. W. Eisinger, V. Fan, S. Fewer, J. Furin, J. D. Goldhaber-Fiebert, G. B. Gomez, S. M. Graham, D. Gupta, M. Kamene, S. Khaparde, E. W. Mailu, E. O. Masini, L. McHugh, E. Mitchell, S. Moon, M. Osberg, T. Pande, L. Prince, K. Rade, R. Rao, M. Remme, J. A. Seddon, C. Selwyn, P. Shete, K. S. Sachdeva, G. Stallworthy, J. F. Vesga, V. Vilc, E. P. Goosby, *Lancet* **2019**, 393, 10178.
- [2] a) D. J. Greenwood, M. S. Dos Santos, S. Huang, M. R. G. Russell, L. M. Collinson, J. I. MacRae, A. West, H. Jiang, M. G. Gutierrez, *Science* **2019**,

- 364, 1279; b) H. E. A. Ahmed, S. K. Ihmaid, A. M. Omar, A. M. Shehata, H. S. Rateb, M. F. Zayed, S. Ahmed, M. M. Elaasser, *Bioorg. Chem.* **2018**, *76*, 332; c) C. J. H. Porter, N. L. Trevaskis, W. N. Charman, *Nature* **2007**, *6*, 231.
- [3] a) R. A. Fisher, B. Gollan, S. Helaine, *Nature* **2017**, *15*, 453; b) M. F. Chellat, L. Raguz, R. Riedl, *Angew. Chem. Int. Ed.* **2016**, *55*, 6600.
- [4] G. Weiss, U. E. Schaible, *Immunol. Rev.* **2015**, *264*, 182.
- [5] a) R. Tandon, M. Nath, *Mini-Rev. Med. Chem.* **2017**, *17*, 549; b) C. Trefzer, H. Skovierova, S. Buroni, A. Bobovska, S. Nenci, E. Molteni, F. Pojer, M. R. Pasca, V. Makarov, S. T. Cole, G. Riccardi, K. Mikušová, K. Johnsson, *J. Am. Chem. Soc.* **2012**, *134*, 912.
- [6] F. Kloss, V. Krchnak, A. Krchnakova, S. Schieferdecker, J. Dreisbach, V. Krone, U. Möllmann, M. Hoelscher, M. J. Miller, *Angew. Chem. Int. Ed.* **2017**, *56*, 2187.
- [7] Reviews: a) M. Sommerfeld, Y. Cui, S. Schmalzfuss, *Eur. J. Pharm. Sci.* **2019**, *128*, 299; b) J. Weers, A. Clark, *Pharm. Res.* **2017**, *34*, 507.
- [8] Reviews: a) D. Wang, C. Yu, L. Xu, L. Shi, G. Tong, J. Wu, H. Liu, D. Yan, X. Zhu, *J. Am. Chem. Soc.* **2018**, *140*, 8797; b) G. M. Keserü, G. M. Makara, *Nature* **2009**, *8*, 203; c) V. J. Venditto, F. C. Szoka, *Adv. Drug Delivery Rev.* **2013**, *65*, 80.
- [9] a) W. Chen, C. A. Glackin, M. A. Horwitz, J. I. Zink, *Acc. Chem. Res.* **2019**, *52*, 1531; b) T. Ellis, M. Chiappi, A. García-Trenco, M. Al-Ejji, S. Sarkar, T. K. Georgiou, M. S. P. Shaffer, T. D. Tetley, S. Schwander, M. P. Ryan, A. E. Porter, *ACS Nano* **2018**, *12*, 5228; c) S. Valetti, X. Xia, M. Andersson, A. Feiler, S. Valetti, J. Costa-Gouveia, P. Brodin, M. F. Bernet-Camard, A. Feiler, *Nanomedicine* **2017**, *12*, 831; d) P. Leidinger, J. Treptow, K. Hagens, J. Eich, N. Zehethofer, D. Schwudke, W. Öhlmann, H. Lünsdorf, O. Goldmann, U. E. Schaible, K. E. J. Dittmar, C. Feldmann, *Angew. Chem. Int. Ed.* **2015**, *54*, 12597.
- [10] a) V. J. Venditto, F. C. Szoka, *Adv. Drug Delivery Rev.* **2013**, *65*, 80; b) Y. Wang, Y. Yan, J. Cui, L. Hosta-Rigau, J. K. Heath, E. C. Nice, F. Caruso, *Adv. Mater.* **2010**, *22*, 4293; c) A. Fahr, X. Liu, *Expert Opin. Drug Delivery* **2007**, *4*, 403; d) C. A. Lipinski, F. Lombardo, B. W. Dominy, P. J. Feeney, *Adv. Drug Delivery Rev.* **2001**, *46*, 3.
- [11] a) S. Wolf, C. Feldmann, *Angew. Chem. Int. Ed.* **2016**, *55*, 15728; b) J. Jung-König, M. Sanhaji, R. Popescu, C. Seidl, E. Zittel, U. Schepers, D. Gerthsen, I. Hilger, C. Feldmann, *Nanoscale* **2017**, *9*, 8362; c) V. Rein, E. Zittel, K. Hagens, N. Redinger, U. Schepers, H. Mehlhorn, U. Schaible, C. Feldmann, *Adv. Funct. Mater.* **2019**, *29*, 1900543.
- [12] a) S. Pescina, G. Garrastazu, E. del Favero, V. Rondelli, L. Cantu, C. Padula, P. Santi, S. Nicoli, *Eur. J. Pharm. Sci.* **2018**, *125*, 223; b) A. Kogan, D. E. Shalev, U. Raviv, A. Aserin, N. Garti, *J. Phys. Chem. B* **2009**, *113*, 10669.
- [13] A. Maleki, H. Kettiger, A. Schoubben, J. M. Rosenholm, V. Ambrogio, M. Hamidi, *J. Controlled Release* **2017**, *262*, 329.
- [14] G. A. Parks, *Chem. Rev.* **1965**, *65*, 177.
- [15] a) B. L. Neumeier, M. Khorenko, F. Alves, O. Goldmann, J. Napp, U. Schepers, H. M. Reichardt, C. Feldmann, *ChemNanoMat* **2019**, *5*, 24; b) J. A. M. van der Houwen, G. Cressey, B. A. Cressey, E. Valsami-Jones, *J. Cryst. Growth* **2003**, *249*, 572.

Manuscript received: July 22, 2020

Revised manuscript received: October 23, 2020

Accepted manuscript online: October 28, 2020

Version of record online: November 27, 2020